2D WSe$_2$/MoS$_2$ van der Waals heterojunction photodiode for visible-near infrared broadband detection ⊘

Hyo Sun Lee; Jongtae Ahn; Wooyoung Shim; Seongil Im; Do Kyung Hwang

Check for updates

View Online

Export Citation

Articles You May Be Interested In

P-doping and efficient carrier injection induced by graphene oxide for high performing WSe$_2$ rectification devices

Appl. Phys. Lett. (March 2016)

A WSe$_2$/MoSe$_2$ heterostructure photovoltaic device

Appl. Phys. Lett. (September 2015)

Phase-transition modulated, high-performance dual-mode photodetectors based on WSe$_2$/VO$_2$ heterojunctions

Appl. Phys. Rev. (December 2019)

30 March 2025 07:54:23

AIP Publishing
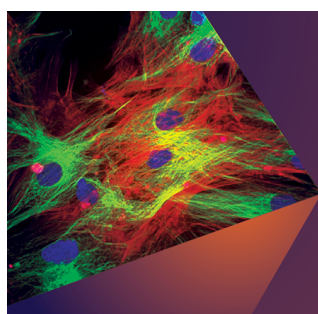
Applied Physics Letters

2D WSe$_2$/MoS$_2$ van der Waals heterojunction photodiode for visible-near infrared broadband detection

Hyo Sun Lee,[1,2,a)] Jongtae Ahn,[1,3,a)] Wooyoung Shim,[2] Seongil Im,[3] and Do Kyung Hwang[1,4,b)]

[1]Center of Opto-Electronic Materials and Devices, Post-Silicon Semiconductor Institute Korea Institute of Science and Technology (KIST), Seoul 02792, South Korea
[2]Department of Materials Science and Engineering, Yonsei University, Seoul 03722, South Korea
[3]Institute of Physics and Applied Physics, Yonsei University, Seoul 03722, South Korea
[4]Division of Nano & Information Technology, KIST School, Korea University of Science and Technology (KUST), Seoul 02792, South Korea

Two dimensional (2D) layered van der Waals (vdW) atomic crystals are an important class of emerging materials due to their unique physical properties. In particular, the nature of dangling–bond–free surfaces in 2D vdW materials enables the formation of heterojunctions without the constraint of atomic lattice match. Here, we report on a 2D WSe$_2$/MoS$_2$ multilayer van der Waals heterojunction PN diode and its application for visible-near infrared broadband detection. The WSe$_2$/MoS$_2$ PN diode shows excellent performance with an ideality factor of 1.5 and a high rectification (ON/OFF) ratio of over 10^6. This PN diode exhibits spectral photo-responses from the ultraviolet (405 nm) region to the near infrared (808 nm) region with obvious photovoltaic behaviors (very clear open circuit voltage and short circuit current). In addition to the static behavior, photocurrent switching behaviors are clearly observed under periodic illuminations at up to 1 KHz. The device shows a linear response within the optical power density range of 10^{-5} W cm^{-2} to 1 W cm^{-2} and a linear dynamic range is estimated to be 123 dB. *Published by AIP Publishing.* https://doi.org/10.1063/1.5042440

Since the discovery of graphene, various two dimensional (2D) layered van der Waals (vdW) materials have been synthesized, and their unique and interesting physical properties have been reported.[1–8] Of the many unique physical properties of 2D vdW materials, the nature of dangling–bond–free surfaces enables the formation of heterostructures without the constraint of atomic lattice match.[2,9] Such vdW heterostructures not only herald opportunities for conducting fundamental nanoscience studies[6] but also offer a versatile platform for diverse nanoscale electronic/optoelectronic applications.[10–13]

In general, PN junction diodes are as important as field-effect transistors (FETs), which can be basic building blocks for electronic or optoelectronic systems. The vdW heterostructures based on 2D semiconductors can allow a facile implementation of heterojunction PN diodes. Such vdW heterojunction PN diodes have great potential for photodetection, which play an important role in many optoelectronic applications of video imaging, remote sensing, optical communications, and display technology. Despite introductions of several 2D vdW heterojunction PN diodes,[14–21] the p-WSe$_2$/n-MoS$_2$ heterojunction still remains one of the most promising structures due to its relatively high carrier mobility, high light absorbance, and well defined current rectification effects. Indeed, the WSe$_2$/MoS$_2$ heterojunction has been extensively studied.[22–28] However, most of the WSe$_2$/MoS$_2$ heterojunction diodes were fabricated on the SiO$_2$/Si substrate due to additional gate bias support. In addition, quasi-neutral

regions besides junctions existed between two electrode terminals, leading to large series resistance which hinders proper photovoltaic behavior.

In this study, we have fabricated a 2D WSe$_2$/MoS$_2$ multilayer vdW heterojunction PN diode on a glass substrate where a Pt electrode for the WSe$_2$ contact was placed underneath the heterojunction for reducing the quasi-neutral region. Such a vertical contact of Pt/WSe$_2$ is advantageous to reduce the quasi-neutral region, resulting in proper photovoltaic behaviors.[26] The WSe$_2$/MoS$_2$ PN diode shows excellent performance with an ideality factor of 1.5 and a high rectification (ON/OFF) ratio of over 10^6 without any additional bias support. The photodetection properties of the WSe$_2$/MoS$_2$ PN diode were thoroughly characterized. This PN diode exhibited broadband spectral photo-responses from the ultraviolet region (405 nm) to the near infrared (NIR) region (808 nm) with obvious photovoltaic behaviors (very clear open circuit voltage and short circuit current). In addition to the static behavior, photocurrent switching behaviors were clearly observed under periodic illuminations at up to 1 KHz. The device showed a linear response within the optical power density range of 10^{-5} W cm^{-2} to 1 W cm^{-2}, and a linear dynamic range (LDR) was estimated to be 123 dB.

We used our customized direct imprint method to stack two different kinds of nanoflakes. In the first step, a Pt (10 nm) bottom electrode was patterned on the glass substrate (Eagle XG) by DC magnetron sputtering, photolithography, and the lift-off method. Then, a WSe$_2$ nanoflake was mechanically exfoliated by the PDMS (polydimethylsiloxane) stamp and transferred onto Pt for the p-type ohmic-like contact. Subsequently, a MoS$_2$ nanoflake was exfoliated in

a)H. S. Lee and J. Ahn contributed equally to this work.
b)Electronic mail: dkhwang@kist.re.kr

the same way as the WSe_2 flake and transferred to be partially overlaid on WSe_2; then, a vertical PN heterojunction formed. Finally, a Ti (25 nm)/Au (25 nm) top electrode was deposited on MoS_2 and patterned in the same way of lithography and lift-off processes as done for the Pt electrode. Figures 1(a) and 1(b) show a three-dimensional (3D) scheme and optical microscopy (OM) image of the 2D WSe_2/MoS_2 heterojunction PN diode. The Pt electrode for the WSe_2 contact was placed underneath the heterojunction for reducing the quasi-neutral region, as shown in Fig. 1(b). The heterojunction area is estimated to be 326 μm^2. According to the step-height profiles obtained from an atomic force microscope (AFM) as shown in Fig. 1(c), the thicknesses of WSe_2 and MoS_2 multilayers were estimated to be $\sim$25 nm and $\sim$18 nm, respectively, whereas the insets show surface topographic images. Before characterization of the WSe_2/MoS_2 heterojunction diode, in order to confirm the ohmic-like contact of WSe_2/Pt and MoS_2/Ti, we have fabricated Pt/WSe_2/Pt and Ti/MoS_2/Ti devices on SiO_2/Si substrates. Although there might be barriers, these devices showed nearly linear current-voltage characteristics without additional back gate bias, as shown in Figs. 1(d) and 1(e). In addition, the rectification behaviors were not observed in both Pt/WSe_2/Pt and Ti/MoS_2/Ti devices.

All static electrical and photoelectric measurements of our device were performed with a semiconductor parameter analyzer (Agilent 4155 B) in the dark and under laser diodes (LDs, purchased from Thorlabs, Inc.): NIR1 (980 nm), NIR2 (808 nm), red (638 nm), green (532 nm), and ultraviolet (405 nm). Dynamic ON/OFF photoswitching behaviors were observed using a function generator (Tekronix AFG3022B) to operate the LDs.

Figure 2(a) shows the current–voltage (*I–V*) characteristics of the WSe_2/MoS_2 heterojunction diode. This heterojunction diode showed typical PN junction diode behavior without any additional bias support, and the ideal factor was estimated to be 1.5. While the leakage current under reverse bias (from -1 V to -3 V) was extremely low on the order of 10^{-12} A, the maximum ON current (I_{ON}) appeared to be on the order of 10^{-6} A, resulting in the very high rectification (ON/OFF) ratio of over 10^6. Dynamic current rectification behaviors were also examined. When input square waves of $V_{IN} = \pm 1$ V at 10 Hz and 100 Hz were applied, obviously rectified output currents were observed, as shown in Figs. 2(b) and 2(c). Considering the *I-V* curve shape, an ideality factor of 1.5, a high rectification (ON/OFF) ratio of over 10^6, and dynamic rectification behaviors, our WSe_2/MoS_2 heterojunction diode showed superior electrical performance even without additional gate bias. The above electrical parameters are comparable to or even better than those of 2D vdW heterojunction PN diodes previously reported in the literature studies.[14,17,21,25–28]

In order to investigate the photodiode properties, the photo-induced *I–V* characteristics were measured using NIR1 (980 nm), NIR2 (808 nm), red (638 nm), green (532 nm), and ultraviolet (405 nm) LDs as light sources. Optical power densities of all LDs were set to 100 mW cm^{-2}. Figures 3(a) and 3(b) display dark and photo-induced *I–V* characteristics of the WSe_2/MoS_2 heterojunction diode on a logarithmic scale and a liner scale under LD illuminations. This PN diode clearly exhibited broadband spectral photo-responses in the 405–808 nm range. In addition, the device also responded to NIR (980 nm) light even though the response is weak. Because WSe_2 and MoS_2 multilayers have an energy bandgap of approximately 1.2–1.3 eV, our WSe_2/MoS_2 heterojunction can respond to above broadband lights. It is worth noting that the WSe_2/MoS_2 heterojunction diode also showed photovoltaic (PV) behaviors, as shown in Fig. 3(b). A very clear open circuit voltage (V_{oc}) of 0.3–0.4 V and a short circuit current (I_{SC}) of 10–40 nA were observed, indicating that our device also has the potential for use in solar cells or photovoltaic type detectors. Spectral responsivities as a function of illumination wavelengths were directly extracted from photo-induced *I–V* curves at V = 0 V (short circuit condition, photovoltaic mode) and V = -3 V (reverse bias condition) and are plotted in Fig. 3(c). Both responsivities under the short circuit condition (photovoltaic mode) and the reverse bias condition followed the same trend: the peak responsivities of 0.11 A/W (short circuit condition) and 0.17 A/W (reverse bias condition) were observed under green LD illumination. Spectral responsivity is affected by several factors such as absorbance, penetration depth of light, charge collection efficiency, and so on. The highest responsivity under green LD illumination may be a result of competition between the absorbance of MoS_2/WSe_2 and the penetration depth of light.[13,26] In order to examine the batch-to-batch

(a)

(b)

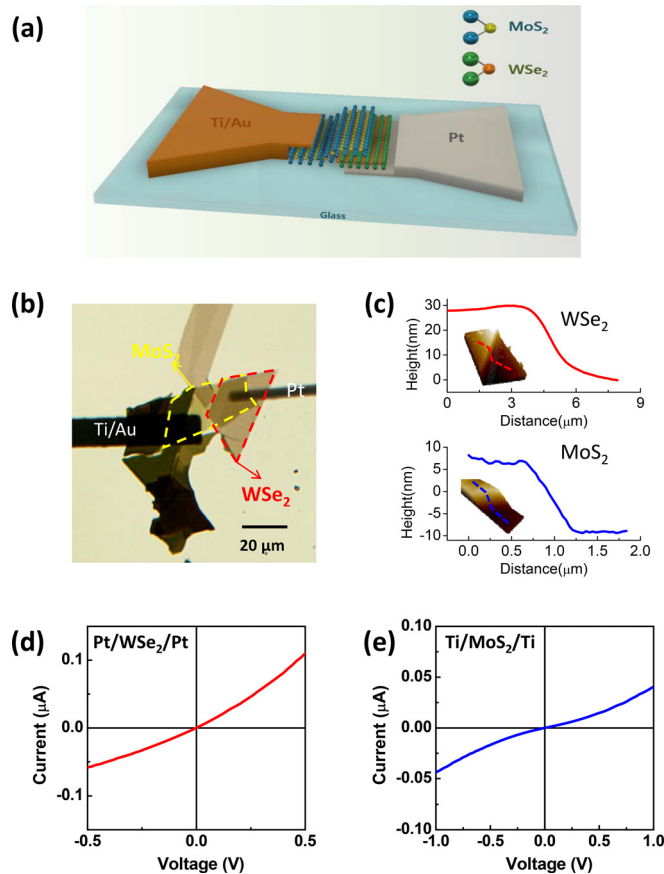**(c)**

(d) Pt/WSe_2/Pt

(e) Ti/MoS_2/Ti

FIG. 1. (a) Schematic 3D view and (b) OM images of the WSe_2/MoS_2 heterojunction. (c) The AFM step-height profiles and surface topographic images of WSe_2 and MoS_2 nanosheets. (d) and (e) Current–voltage (*I-V*) characteristics of Pt/WSe_2/Pt and Ti/MoS_2/Ti devices on SiO_2/Si substrates to examine Pt/WSe_2 and Ti/MoS_2 contacts.
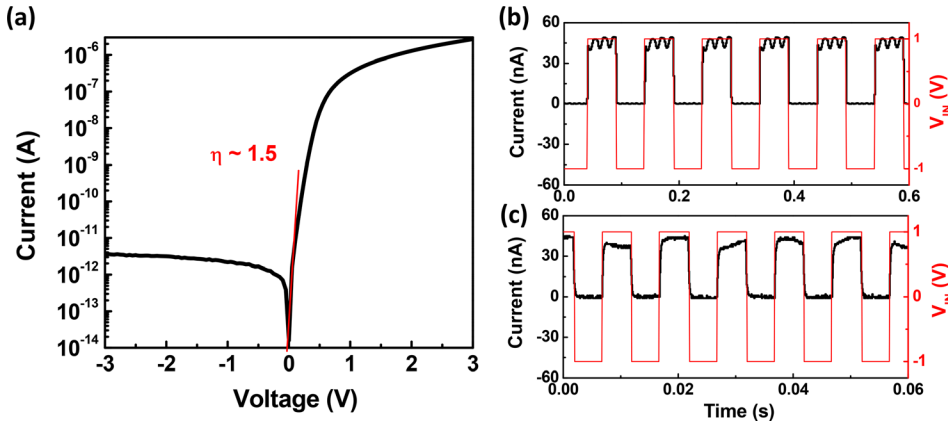
FIG. 2. (a) *I-V* characteristics on the logarithmic scale obtained from the WSe$_2$/MoS$_2$ heterojunction diode. Dynamic current rectification behaviors at (b) 10 Hz and (c) 100 Hz input square waves of $V_{IN} = \pm 1$ V.
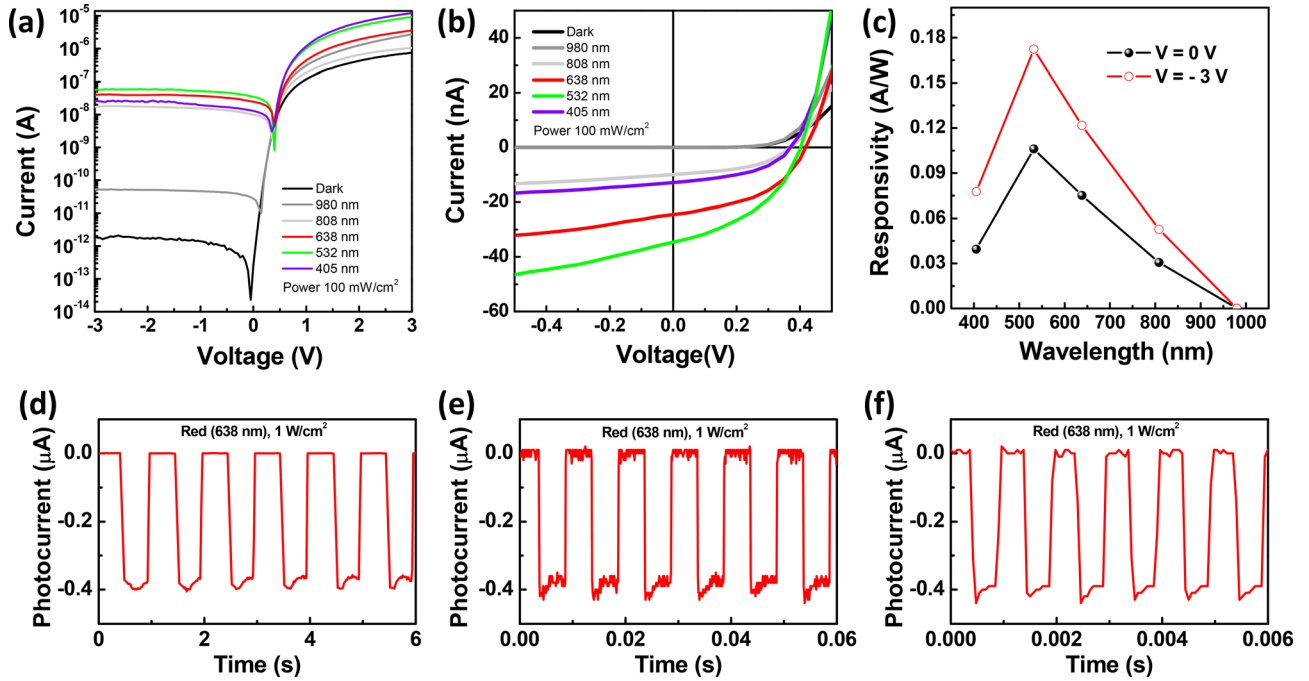

FIG. 3. Dark and photo-induced *I–V* characteristics of the WSe$_2$/MoS$_2$ heterojunction photodiode on (a) logarithmic scale and (b) liner scale under NIR (980 and 808 nm), red (638 nm), green (532 nm), and violet (405 nm) LD illuminations. (c) Spectral responsivity characteristics as a function of illumination wavelengths. Responsivity values were extracted at V = 0 V (short circuit condition, photovoltaic mode) and V = −3 V (reverse bias condition). Temporal photocurrent characteristics of devices at V = 0 V under periodic red LD illumination at (d) 1 Hz, (e) 100 Hz, and (f) 1 kHz.

uniformity of WSe$_2$/MoS$_2$ heterojunction diodes, two more bathes (batch 1 and batch 2) were characterized. Very similar spectral *I-V* curves and responsivities were observed (see Fig. S1 in the supplementary material).

In addition to the photostatic behaviors, photocurrent switching behaviors were also measured, as shown in Figs. 3(d)–3(f). The device showed obvious photocurrent switching behaviors at V = 0 V (short circuit condition) and negligible changes under periodic red LD illuminations at up to 1 kHz, indicating that the WSe$_2$/MoS$_2$ photodiode can perform at least 1 kHz operation.

Another important characteristic of the photodetector is the linearity of photocurrent depending on illumination powers. In order to examine such a linearity of the WSe$_2$/MoS$_2$ photodiode, the green LD light (532 nm) was chosen because the highest photocurrent (peak responsivity) was obtained. Figures 4(a) and 4(b) show dark and selected photo-induced *I–V* characteristics on a logarithmic scale and a liner scale at different green LD illumination power densities ranging

from 3.1×10^{-5} W cm^{-2} to 1.55 W cm^{-2}. In this measured range of optical powers, the photodiode exhibited obvious photocurrents. From the above photo-induced *I–V* curve, photocurrents at V = 0 V (short circuit condition) and V = −3 V (reverse bias condition) as a function of optical illumination power densities are plotted in Fig. 4(c). The relationship between photocurrent and optical power follows a power law given by

$$I_{ph} = AP^{\alpha}, \qquad (1)$$

where I$_{ph}$ is the photocurrent, A is a constant, P is the laser power density, and α is calculated by exponential fitting to be 0.95 (short circuit condition) and 0.92 (reverse bias condition). Both photocurrents under short circuit and reverse bias were linearly proportional to laser power densities (α is 0.95 and 0.92) and showed no indication of saturation over the measured range of laser powers, indicating that the absorption of light and the generation/collection of carriers are balanced. Laser power dependent responsivities are also plotted
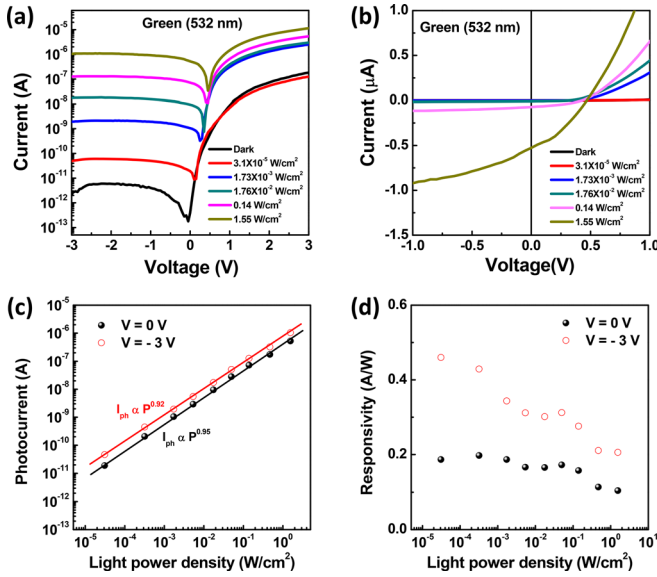
FIG. 4. Dependence of photo-response on green LD illumination intensity. Dark and selected photo-induced I–V characteristics on (a) logarithmic scale and (b) liner scale at different green LD illumination intensities. (c) Photocurrent and (d) responsivity at V = 0 V (short circuit condition, photo-voltaic mode) and V = −3 V (reverse bias condition) versus optical illumination power density.

in Fig. 4(d). The responsivities as a function of laser power intensities can be given by

$$R = \frac{I_{ph}}{P} = \frac{AP^{\alpha}}{P} = AP^{\alpha-1}. \quad (2)$$

α is less than unity, and thus, the responsivities increased with decreasing illumination intensities. The LDR is also a figure-of-merit to evaluate the linearity of photodetectors, which is given by (typically quoted in dB)[29]

$$LDR = 20\log\frac{I_{ph}^*}{I_d}, \quad (3)$$

where I_d is the dark current and I_{ph}^* is the photocurrent, measured at a light intensity of 1.55 W cm^{-2}. LDRs are calculated to be 123 dB (short circuit condition) and 113 dB (reverse bias condition). We also characterized the linearity of a different batch (batch 2). As expected, very similar behaviors were observed. α and LDRs are estimated to be 0.99 and 129 dB under the short circuit condition and 0.9 and 119 dB under the reverse bias condition (see Fig. S2 in the supplementary material).

According to the above photodiode results, our WSe$_2$/MoS$_2$ PN diode showed broad spectral responses with obvious photovoltaic behaviors (very clear open circuit voltage and short circuit current), fast and reproducible photocurrent switching behaviors at 1 KHz (the rising and falling times less than 0.1 ms), and excellent linearity (α of 0.95 and 0.92). Such photodiode performance parameters are also comparable to or even much better than those of 2D photodiodes previously reported in the literature studies.[14,17,21,25–28] In particular, LDRs of 123 dB and 129 dB are comparable to commercial Si (120 dB) and InGaAs photodetectors (66 dB).[29]

In summary, we have fabricated the 2D WSe$_2$/MoS$_2$ multilayer van der Waals heterojunction PN diode that showed excellent performance with an ideality factor of 1.5 and a high rectification (ON/OFF) ratio of over 10^6. This PN diode exhibited broadband spectral photo-responses from the ultraviolet region (405 nm) to the NIR region (808 nm) with the responsivity reaching 0.17 A/W (green, 532 nm). Obvious photovoltaic behaviors under each LD illumination were also observed. In addition to the static behavior, fast and reproducible photocurrent switching behaviors were clearly observed under periodic red LD illuminations at up to 1 KHz. Finally, we examined the linearity of the WSe$_2$/MoS$_2$ PN photodiode. The device showed a linear response within the optical power density range of 10^{-5} W cm^{-2} to 1 W cm^{-2} (green LD), and the resultant LDR was estimated to be 123 dB under the short circuit condition. We, thus, conclude that our WSe$_2$/MoS$_2$ heterojunction PN photodiode can be a promising building block to extend to more advanced 2D nano-optoelectronic applications.

See supplementary material for the spectral photo-response behaviors and linearity characteristics of different batches of WSe$_2$/MoS$_2$ PN diodes.

[1]Q. H. Wang, K. Kalantar-Zadeh, A. Kis, J. N. Coleman, and M. S. Strano, Nat. Nanotechnol. **7**, 699 (2012).
[2]A. K. Geim and I. V. Grigorieva, Nature **499**, 419 (2013).
[3]F. H. L. Koppens, T. Mueller, P. Avouris, A. C. Ferrari, M. S. Vitiello, and M. Polini, Nat. Nanotechnol. **9**, 780 (2014).
[4]K. F. Mak and J. Shan, Nat. Photonics **10**, 216 (2016).
[5]D. Xiao, G. B. Liu, W. X. Feng, X. D. Xu, and W. Yao, Phys, Rev, Lett. **108**, 196802 (2012).
[6]H. Y. Yu, G. B. Liu, J. J. Tang, X. D. Xu, and W. Yao, Sci. Adv. **3**, e1701696 (2017).
[7]Y. L. Wang, L. F. Li, W. Yao, S. R. Song, J. T. Sun, J. B. Pan, X. Ren, C. Li, E. Okunishi, Y. Q. Wang *et al.*, Nano Lett. **15**, 4013 (2015).
[8]S. Lee, Y. T. Lee, S. G. Park, K. H. Lee, S. W. Kim, D. K. Hwang, and K. Lee, Adv. Electron. Mater. **4**, 1700563 (2018).
[9]D. Jariwala, T. J. Marks, and M. C. Hersam, Nat. Mater. **16**, 170 (2017).
[10]D. Kufer, I. Nikitskiy, T. Lasanta, G. Navickaite, F. H. L. Koppens, and G. Konstantatos, Adv. Mater. **27**, 176 (2015).
[11]N. J. Huo, S. Gupta, and G. Konstantatos, Adv. Mater. **29**, 1606576 (2017).
[12]C. Hu, D. D. Dong, X. K. Yang, K. K. Qiao, D. Yang, H. Deng, S. J. Yuan, J. Khan, Y. Lan, H. S. Song *et al.*, Adv. Funct. Mater. **27**, 1603605 (2017).
[13]Y. T. Lee, P. J. Jeon, J. H. Han, J. Ahn, H. S. Lee, J. Y. Lim, W. K. Choi, J. D. Song, M. C. Park, S. Im *et al.*, Adv. Funct. Mater. **27**, 1703822 (2017).
[14]Y. Deng, Z. Luo, N. J. Conrad, H. Liu, Y. Gong, S. Najmaei, P. M. Ajayan, J. Lou, X. Xu, and P. D. Ye, ACS Nano **8**, 8292 (2014).
[15]L. Ye, H. Li, Z. F. Chen, and J. B. Xu, ACS Photonics **3**, 692 (2016).
[16]G. Lee, S. J. Pearton, F. Ren, and J. Kim, ACS Appl. Mater. Interfaces **10**, 10347 (2018).
[17]K. A. Zhang, T. N. Zhang, G. H. Cheng, T. X. Li, S. X. Wang, W. Wei, X. H. Zhou, W. W. Yu, Y. Sun, P. Wang *et al.*, ACS Nano **10**, 3852 (2016).
[18]F. Wang, L. Yin, Z. X. Wang, K. Xu, F. M. Wang, T. A. Shifa, Y. Huang, C. Jiang, and J. He, Adv. Funct. Mater. **26**, 5499 (2016).
[19]Y. Chen, X. D. Wang, G. J. Wu, Z. Wang, H. H. Fang, T. Lin, S. Sun, H. Shen, W. D. Hu, J. L. Wang *et al.*, Small **14**, 1703293 (2018).

[20]X. Zhou, X. Z. Hu, S. S. Zhou, H. Y. Song, Q. Zhang, L. J. Pi, L. Li, H. Q. Li, J. T. Lu, and T. Y. Zhai, Adv. Mater. **30**, 1703286 (2018).

[21]K. Murali, M. Dandu, S. Das, and K. Majumdar, ACS Appl. Mater. Interfaces **10**, 5657 (2018).

[22]M. M. Furchi, A. Pospischil, F. Libisch, J. Burgdorfer, and T. Mueller, Nano Lett. **14**, 4785 (2014).

[23]M. Y. Li, Y. M. Shi, C. C. Cheng, L. S. Lu, Y. C. Lin, H. L. Tang, M. L. Tsai, C. W. Chu, K. H. Wei, J. H. He *et al.*, Science **349**, 524 (2015).

[24]C. H. Lee, G. H. Lee, A. M. van der Zande, W. C. Chen, Y. L. Li, M. Y. Han, X. Cui, G. Arefe, C. Nuckolls, T. F. Heinz *et al.*, Nat. Nanotechnol. **9**, 676 (2014).

[25]P. J. Jeon, S.-W. Min, J. S. Kim, S. R. A. Raza, K. Choi, H. S. Lee, Y. T. Lee, D. K. Hwang, H. J. Choi, and S. Im, J. Mater. Chem. C **3**, 2751 (2015).

[26]J. Ahn, P. J. Jeon, S. R. A. Raza, A. Pezeshki, S. W. Min, D. K. Hwang, and S. Im, 2D Mater. **3**, 045011 (2016).

[27]M. X. Sun, Q. Y. Fang, D. Xie, Y. L. Sun, J. L. Xu, C. J. Teng, R. X. Dai, P. Yang, Z. X. Li, W. W. Li *et al.*, Adv. Electron. Mater. **3**, 1600502 (2017).

[28]M. Y. Li, J. Pu, J. K. Huang, Y. Miyauchi, K. Matsuda, T. Takenobu, and L. J. Li, Adv. Funct. Mater. **28**, 1706860 (2018).

[29]L. T. Dou, Y. Yang, J. B. You, Z. R. Hong, W. H. Chang, and G. Li, Nat. Commun. **5**, 5404 (2014).